Published in final edited form as:
J Proteome Res. 2011 March 4; 10(3): 1343–1352. doi:10.1021/pr101075e.

Analysis of phosphotyrosine signaling in glioblastoma identifies STAT5 as a novel downstream target of ΔEGFR

Vaibhav Chumbalkar[*,1], **Khatri Latha**[*,1], **YeoHyeon Hwang**[1], **Rebecca Maywald**[1], **Lauren Hawley**[1], **Raymond Sawaya**[1], **Lixia Diao**[2], **Keith Baggerly**[2], **Webster K. Cavenee**[3], **Frank B. Furnari**[3], and **Oliver Bogler**[1,4,5]

[1]Department of Neurosurgery, The University of Texas MD Anderson Cancer Center, Houston TX

[2]Department of Bioinformatics and Computational Biology, The University of Texas MD Anderson Cancer Center, Houston TX

[3]Ludwig Institute for Cancer Research, San Diego Branch, La Jolla CA

[4]Department of Neuro-Oncology, The University of Texas MD Anderson Cancer Center, Houston TX

[5]Graduate School of Biomedical Sciences, The University of Texas MD Anderson Cancer Center, Houston TX

Abstract

An in-frame deletion mutation in Epidermal Growth Receptor (EGFR), ΔEGFR is a common and potent oncogene in glioblastoma (GBM), promoting growth and survival of cancer cells. This mutated receptor is ligand independent and constitutively active. Its activity is low in intensity and thought to be qualitatively different from acutely ligand stimulated wild type receptor implying that the preferred downstream targets of ΔEGFR play a significant role in malignancy. To understand the ΔEGFR signal we compared it to that of a kinase-inactivated mutant of ΔEGFR and wild-type EGFR with shotgun phosphoproteomics using an electron-transfer dissociation (ETD) enabled ion trap mass spectrometer. We identified and quantified 354 phosphopeptides corresponding to 249 proteins. Among the ΔEGFR-associated phosphorylations were the previously described Gab1, c-Met and Mig-6, and also novel phosphorylations including that of STAT5 on Y694/9. We have confirmed the most prominent phosphorylation events in cultured cells and in murine xenograft models of glioblastoma. Pathway analysis of these proteins suggests a preference for an alternative signal transduction pathway by ΔEGFR compared to wild type EGFR. This understanding will potentially benefit the search for new therapeutic targets for ΔEGFR expressing tumors.

Introduction

Aberrant receptor tyrosine kinase activity is implicated in many cancers. One of the most important tyrosine kinase receptors in glioblastoma is EGFR, recently confirmed by a TCGA study [1] where overexpression due to genomic amplification was demonstrated, and found to be associated with mutation of the receptor. The most common mutation EGFRvIII or ΔEGFR is genomic loss of exons 2-7, causing an in-frame deletion of 801 bp in the

Corresponding Author's Contact details: Oliver Bogler, Ph.D Professor of Neurosurgery VP, Global Academic Programs The University of Texas MD Anderson Cancer Center 1515 Holcombe Boulevard, Houston, Texas 77030-4009, USA Phone (713) 745-4438 Fax: 713-563-0003 obogler@mdanderson.org.
*these authors contributed equally.

extracellular domain [2, 3]. ΔEGFR signals constitutively in the absence of ligand and without significant internalization or downregulation [4-7]. The ΔEGFR signal is also approximately 5-to10-fold lower than acutely stimulated wild-type, as measured by tyrosine phosphorylation, and shows a greater sensitivity to loss of even one tyrosine residue in its C-terminus [5, 8, 9]. Therefore, while the wild-type receptor stimulated by EGF transmits a high-intensity, short-duration signal, ΔEGFR produces a low-intensity continuous signal, raising the question of whether their downstream effectors differ. Interestingly, the pattern of tyrosine phosphorylations in the C-terminus of ΔEGFR does not appear to differ markedly from EGFR [5]. Candidate analysis suggests that some elements in the EGFR pathway are activated to a greater degree, or in a more sustained fashion by ΔEGFR, but has not yielded a comprehensive picture. A powerful alternative approach is an unbiased analysis of phosphopeptides by mass spectrometry when their relatively low abundance is overcome by enrichment [10-12]. This approach was used to analyze the impact of medium, high and super-high levels of ΔEGFR in U87 glioma cells, revealing preferential activation of the PI3K pathway over the mitogen-activated protein kinase (MAPK) pathway, and a connection to c-Met [13]. Here we present a complementary study using two different cell lines, LNZ308 and LN428, and including novel comparisons of the ΔEGFR signal with a kinase inactive ΔEGFR (ΔEGFR-ki) and acutely EGF-stimulated EGFR. We have identified and confirmed a limited number of proteins with higher levels of tyrosine phosphorylation when ΔEGFR is present, including the previously described Gab1, c-Met and Mig-6, and the novel STAT5. We propose a preferred signaling pathway for ΔEGFR that is active in glioma.

Materials and Methods

Cell Culture, Retrovirus Infection, and Transfection.

The human glioblastoma cell lines LNZ308 and LN428 were cultured in DMEM with 10% FBS/2 mM glutamine/100 units/ml penicillin/100 mg/ml streptomycin in 95% air/ 7% CO2 atmosphere at 37°C. Cells were transfected with EGFR, ΔEGFR, ΔEGFR-ki [5] or the vector control in 1726zeoG retrovirus (derivative of 1726zeo [14] with a Gateway destination vector (Invitrogen) cassette in the unique EcoRI site) by Lipofectamine 2000 (Invitrogen) and selected in 50 μg/ml of Zeocin. The cells were routinely grown in DMEM medium with 50 μg/ml of Zeocin. Cell lines were fingerprinted for identity using a PCR-based analysis (GenomeLab Human STR Primer set from Beckman Coulter) which interrogates a set of 12 short tandem repeats (Supplemental Data, Table S3).

Sample preparation for Mass Spectrometry (Cell Lysis and Tryptic Digestion)

The cells were seeded in 150 mm dishes for 24 h reaching approximately 70-80% confluency, then washed with PBS and incubated for 24 h in serum free medium. In some instances the EGFR overexpressing cells were stimulated with EGF (5 ng/ml) for 5 min before lysis. Three biological replicates of all samples were prepared for this study. The cells were scraped with Urea Lysis Buffer (20 mM HEPES pH 8.0, 9 M urea, 1 mM sodium orthovanadate, 2.5 mM sodium pyrophosphate, 1 mM b-glycerophosphate). After incubation on ice for 10 minutes, sonication was done at 15W and the cells were sonicated for three pulses for 30s each, with 2 min on ice between pulses. The lysates were then centrifuged at 20,000 xg for 15 min and the resulting supernatant was then reduced with 4.5 mM of DTT at 60°C for 20 min followed by carboxoamidomethylation with 10 mM iodoacetamide in dark at room temperature for 15 min. Trypsin digestion of the lysates was carried out by diluting the lysates four times with HEPES buffer to final concentration of 20 mM of HEPES and adding trypsin TPCK solution (Worthington Biochemical) to final concentration of 10 μg/ml which was then left at room temperature overnight. Peptides were desalted using Sep-Pak C18 column (Waters Corp), and lyophilized for two days in freeze dry system.

Peptide Immunoprecipitation

Lyophilized peptides were resuspended in Immunnoaffinity Purification (IAP) buffer (50 mM MOPS pH 7.2, 10 mM sodium phosphate, 50 mM NaCl) and transferred to a microfuge tube having phosphotyrosine antibody (Cat No.7902 Phospho-Tyrosine Mouse mAb (P-Tyr-100) Beads, Cell Signaling Technology). IAP was carried out overnight at 4°C. Beads were washed three times with IAP buffer and water. Bound peptides were eluted with 0.15% TFA. Eluted peptides were further purified using ZipTip C18 (Millipore Corp).

Mass Spectrometry

Mass Spectrometry analysis was done using Agilent's 6340 Ion trap System with ETD. This was inline with Agilent's 1200 series HPLC-Chip system. Peptides were resuspended in 3% ACN, 0.1% TFA and loaded onto Agilent's Protein ID chip #2 (40 nl enrichment column, 75 μm × 150 mm analytical column. Stationary phase: 5 mm, C-18 SB-Zorbax, 300A). Peptides were eluted with 150 min, 3-90% step gradient of mobile phase B (0.1% formic acid in Acetonitrile). Mobile phase A being 0.1% formic acid and steps for the gradient are 5-20 min- 15%B, 20-120 min 45% B, 120-140 min 90%B. A high resolution MS scan was done (standard enhanced mode – 8100 m/z / sec) followed by data dependent MS/MS at higher scan speed (Ultrascan mode – 26000 m/z / sec). For data dependent MS/MS, four peptides preferably with more than a double charge were selected in each scan cycle. This analysis was done in both collision induced dissociation (CID) and electron transfer dissociation (ETD) mode, as separate runs. For CID mode, MS3 was triggered with neutral loss of 49,58,98 and 116 amu.

Database Analysis

The tandem mass spectra obtained were extracted using Spectrum Mill MS Proteomics Bench software version A.03.03.082 (Agilent Technologies) with the following parameters selected: parent mass range: 600-10000, merge scans: within ± 15 sec. and ± 1.4 m/z, also whenever MS3 was triggered it was merged with MS2 with 5× intensity. The database search was done against NCBI RefSeq human subset (having 37442 sequences) downloaded in September 2008 using Spectrum Mill software. We used Spectrum Mill because it is integrated with our MS platform and has shown to perform well when searching either ETD or combined CID/ETD data [12, 15, 16]. An error of 4 Da in parent mass (maximum error observed for parent mass was 1.303) and 0.8 Da in fragment mass was allowed and 2 missed cleavages were allowed with trypsin selected as protease. The database search was carried out in forward as well as reverse modes. Carbamidomethylation of cysteine was selected as fixed modification. Variable modifications searched were phosphorylation of serine, threonine and tyrosine with oxidation of methionine and pyroglutamate at the N- terminus. Stepwise validation was done first using the default criteria in the Spectrum Mill software and then by criteria described earlier [12]. In short after default validation by Spectrum Mill, peptides were scored in based on charge as follows, for 5+ score of more than 14, for +4 more than 13, for +3 more than 9 and for +2 more than 7. A small number of lower-scoring peptides with phosphorylation were validated after manually inspecting spectra if the first hit matched with the same peptide and modification in another run with same retention time (± 1 min). For assignment of PTM, in addition to Spectrum Mill score all the spectra are manually inspected and assignment confirmed (see supplementary material – annotated spectra).

Quantification of phosphopeptides

Agilent's Data Analysis software, built for the 6300 series Ion Trap LC/MS, version 3.4, was used to generate m/z xml files that contained the raw data to be used for statistical treatment. The complete LC-MS data set comprised three replicates of each of four modifications/

conditions (serum starved ΔEGFR, serum starved ΔEGFR-ki, serum starved EGFR, and serum starved EGFR stimulated with EGF), in 2 cell lines (LN428 and LNZ308), and analyzed by 2 dissociation modes (CID and ETD), for 3*4*2*2=48 measurements in all. Cell line is confounded with day, but the run order was randomized so that runs of different lines would be interleaved. One run for EGFR+EGF/LNZ308/ETD failed so only two replicates were available for that combination.

Information of the identified phosphopeptides was used further to extract relevant data from all the samples as described below. We took the logical union of the sets of distinct peaks identified for each sample, matching peaks having the same Sequence, MH+, and charge state. We defined a "tolerance window" for each peak using the observed range of elution times plus or minus 15 seconds on one axis, and the observed range of m/z values plus or minus 1.4 Da/charge units on the other. This process identified 514 peaks in the entire data set. In order to quantify the peaks, we read the mzXML files into the free statistical software package R [17] for analysis, using the caMassClass library (ver 1.6). The data were normalized to total ion current (TIC) in two steps. First, a curve of MS-level 1 TIC values as a function of elution time was obtained for each sample and smoothed using loess. These curves were then scaled to have the same overall area (the median of the initial areas), and the average of these scaled TIC curves was then assembled on a point-by-point basis for use as a target. Second, individual MS-level one readings were scaled so that their TIC values would match the target value for the corresponding elution time. For each peak/sample combination, the scaled MS-level 1 counts falling in the tolerance window for the peak were extracted and summed, and this sum used as the quantification for that sample. This process returned a 514 by 47 matrix of peak quantifications, which we log-transformed (base 2) for further analysis. For statistical modeling we performed ANOVA on a peak-by-peak basis, using models with main effect terms for modification/condition, fragmentation mode and run date (cell line is confounded within this last), and interaction terms for modification/condition by dissociation mode, modification/condition by cell line, and dissociation mode by cell line. This filtered out most of the nuisance sources of variation and gave mean squared error estimates for paired contrasts. The phosphopeptides of most interest to us are those showing differential expression across modification/condition. Specifically, we focused on three contrasts: mutant ΔEGFR minus ΔEGFR-ki, ΔEGFR minus EGFR, and EGFR minus EGFR+EGF. We performed paired t-tests for each of the contrasts, using variance estimates (and degrees of freedom for the t-tests) drawn from the ANOVA models above. To correct for multiple testing, we fit the distribution of p-values from each set of t-tests using a beta-uniform mixture (BUM) model [18], which let us estimate false discovery rates (FDRs). These p-value distributions were largely flat with a spike of small p-values, suggesting there were a small number of phosphopeptides showing differential expression. The "top 10" lists for each contrast never had FDRs below 30% (about 3 misses out of 10), so we confirmed these in the spectra visually.

Co-immunoprecipitation assay and immunoblotting assays

Protein concentration was estimated using the Pierce BCA kit (Thermo Scientific) and 20 μg protein was loaded on NuPAGE 4-12% Bis-Tris gels or NuPage 3-8% Tris-Acetate gels (Invitrogen Inc.) for immunoblotting. All primary antibodies used in this study were from Cell Signaling Technologies, except anti-STAT5, which was from Santa Cruz Biotechnology, Inc. Secondary antibody used was goat-anti rabbit from Pierce (Thermo Scientific).

For the co-immunoprecipitation assay, total lysates were incubated with either anti-cMet or anti-Mig6 antibodies under gentle shaking at 4°C overnight. Complexes were collected on Protein G Agarose (Santa Cruz Biotechnology). Beads were washed three times with RIPA

buffer and two times with PBS. The immunoprecipitation complexes were resolved by NuPage gels and subjected to immunoblotting analysis.

Animal Experiment

All the animal procedures were approved by the Institutional Animal Care and Use Committee (IACUC) of MD Anderson Cancer Center. Nude mice were injected with 4×10^5 cells of (U87MG-vector control , U87MG ΔEGFR and U87MG-EGFR) in serum-free DMEM media intracranially using a guide screw previously described [19], and tumors were allowed to grow until animals showed signs of distress. Then animals were sacrificed and tumors were harvested, washed with PBS, and snap frozen and stored at −80°C until used. Lysates were made from the tumor by homogenizing the tumor tissue in the lysis buffer (100 mM Tris–HCl [pH 8], 150 mM NaCl, 1% NP-40, 1 mM EGTA, 1 mM EDTA, 0.5% Na deoxycholate, 0.1% SDS, 1 mM PMSF, aprotinin and leupeptin, 1 μg/mL each) using a glass homogenizer on ice. Lysates were further processed for western blotting, as described above.

Results

To identify tyrosine phosphorylations that are induced by ΔEGFR, two glioma cell lines, LNZ308 and LN428, were engineered to express ΔEGFR, a kinase inactive mutant of ΔEGFR (ΔEGFR-ki) or EGFR. All cells were serum starved, and some EGFR-overexpressing cultures also acutely stimulated with EGF (EGFR+EGF; 10 ng/ml for 10 minutes). Analysis of parallel cultures showed that ΔEGFR signaled in the absence of ligand, that ΔEGFR-ki showed no signal, and that EGFR responded to EGF, as expected (Fig. 1A). Furthermore, in PTEN-null LNZ308 cells significant activity was seen in the PI3K pathway, as measured by pAkt, pS6K and pS6, regardless of whether cells expressed ΔEGFR or were stimulated by EGF, again as expected. In contrast, LN428 cells, which are PTEN wild-type, showed regulation of the PI3K pathway evident in pAkt and pS6 levels, which were low unless elevated by ΔEGFR or EGF stimulation, confirming the functioning of the PTEN protein in these cells. Cell lysates were trypsinized and the peptides immunoprecipitated with anti-phosphotyrosine antibody (pTyr-100 PhosphoScan) and analyzed by LC-MS/MS mass spectrometry using methods to maximize the capture of post-translational modifications (Fig. 1B; for details see Methods). Data from both cell lines were combined for phosphoproteomics analysis to allow identification of signaling not predicated on PTEN status, as one line is PTEN-null and the other PTEN wild-type.

In total we identified 433 proteins with 772 peptides out of which 249 proteins corresponding to 354 peptides showed tyrosine phosphorylation (Supplemental Data, Table S1). We performed label-free quantification and statistical analysis, using the raw MS data, resulting in a list of 30 phosphorylations that were significantly different ($p < 0.01$ by ANOVA analysis) between ΔEGFR vs ΔEGFR-ki, ΔEGFR vs EGFR or EGFR+EGF vs EGFR (Table 1; of the 30 phosphorylations 27 were on single tyrosines, and 3 were tyrosine phosphorylations that occurred with others; for complete information see Supplemental Data, Table S1).

It has been previously reported that adding ETD fragmentation to the more standard CID method increases total identification of peptides in large-scale experiments and that this approach is therefore useful when identifying relatively rare post-translational modifications such as phosphorylation [12, 20, 21]. We identified additional 16% unique phosphopeptide ions in ETD mode, and 35% of the total unique phosphopeptide ions in our study were identified with ETD mode (Table 2). Unique phosphopeptide is defined by its sequence, charge and

the modification(s) present on that peptide. We therefore agree with previous findings that combining CID and ETD for the study of phosphorylation offers advantages.

Comparing ΔEGFR to ΔEGFR-ki showed an increase in the intensity of pY peptides derived from the ΔEGFR, including Y1197 and Y1172, as expected (Fig. 2A). We also saw an increase in CDC2, CDK3, GAB1, SHB adaptor protein, Syndecan 2 and Tensin 3 pY residues in ΔEGFR cells when compared to ΔEGFR-ki (Fig. 2A). BCAR1 was the only phosphorylation reduced in cells expressing ΔEGFR compared to ΔEGFR-ki. In the case of CDC2, CDK3, MIG6, Syndecan 2 and Tensin 3, the contrasts in which ΔEGFR was compared to either ΔEGFR-ki or EGFR yielded larger differences than the comparison EGFR+EGF vs EGFR, suggesting that they were modified at higher levels by ΔEGFR (Fig. 2A). When the primary comparison was ΔEGFR vs EGFR the peptides that showed statistically significant changes included three with reductions, derived from Talin 1, SHIP2 and MAPK14 and three with increases, from Tensin 3, MAPK 1 and GPR159 (Fig. 2B). Tyrosine phosphorylations that showed an increase that was predominantly associated with EGF stimulation of EGFR were on MAPK proteins, Tensin 3 and male germ cell associated kinase at Y159 (Table 1).

We confirmed the phosphorylation of c-Met at Y1234 (Fig. 3, Supplemental Data, Table S1). Two different peptides reached statistical significance in the mass spectrometry analysis: peak 207 which showed significance in the comparison ΔEGFR vs EGFR, and peak 71 which showed significance in the comparison ΔEGFR vs ΔEGFR-ki (Fig. 3B). Consistent with this, western blot analysis showed elevated c-Met phosphorylation when ΔEGFR or EGFR was overexpressed in U87 cells (Fig. 3C). The level of pc-Met in U251 or LN428 was less dependent on the presence of activated EGFR signaling, suggesting that the connection between ΔEGFR and cMet is best modeled in U87 cells, where it has been reported previously [13]. Even in U87 cells significant activation of c-Met by overexpressed EGFR stimulated with EGF was observed, a response not analyzed before [13].

Another phosphorylation event that we confirmed was that on Mig6 at Y394 (Fig 4, Supplemental Data, Table S1). Peak 156 showed a significant increase in the comparison ΔEGFR vs ΔEGFRki (Figure 4B). Consistent with this when we immunoprecipitated Mig6 and probed with antiphosphotyrosine antibody in LN428 and LNZ308 cells we found increase Mig6 phosphorylation in cells overexpressing ΔEGFR or EGFR-overexpressing cells that were acutely stimulated with EGF (Fig 4C). This phosphorylation has been reported previously [13], but had not been confirmed by western blot.

Similarly we were able to confirm the increased Gab1 phosphorylation at Y689 (Fig 5 A and B, Supplemental Data, Table1 and S1) which has long been implicated in EGFR signaling [13, 22]. Peak 90 showed increased phosphorylation of Y689 of Gab1 in the comparison ΔEGFR vs ΔEGFRki and also when EGFR overexpressing cells are acutely stimulated with EGF (Figure 5B). When immunoblot analysis for Y689 phosphorylation was performed for U87, LNZ308 and LN428 cells, consistent with our observation in MS analysis we saw increased phosphorylation in ΔEGFR expressing U87 and LN428 cells while in case of LNZ308 levels of p-Gab1 were similar to that in ΔEGFRki (Figure 5C). As expected, Gab1 was phosphorylated by acute EGF stimulation in all three cell lines (Fig 5C).

A phosphorylation not previously shown to be associated with ΔEGFR expression and EGFR activation by EGF was that of Y694/9 on STAT5 (Fig. 6; Y694 on STAT5A and Y699 on STAT5B are homologous residues). Phosphorylation of this site is an obligatory and dominant activation step, and is required for formation of the STAT5 dimer [23]. Peak 186 showed an increase in both ΔEGFR vs ΔEGFR-ki and EGFR+EGF vs EGFR (Fig. 6B). This observation was confirmed in western blots using an antibody specific for pY694/9,

where a strong signal was observed in glioma cells expressing ΔEGFR or overexpressing EGFR and undergoing acute stimulation by EGF (Fig. 6C). Expression of ΔEGFR led to a statistically significant increase in STAT5 phosphorylation in the cell lines used in the initial phosphoproteomic analysis, LNZ308 and LN428, and a trend was observed in U87 and U251 cells (Fig. 6D). EGFR overexpressing cells acutely stimulated with EGF also showed an increase in pSTAT5 (Fig. 6B and C).

To confirm that the signaling events observed in cultured cells also occurred in vivo, we examined intracranial xenografts of U87 (vector control) cells and also U87 cells overexpressing ΔEGFR or EGFR. We detected increased phosphorylation of STAT5, cMet, and increased phosphorylation of Gab1 in tumors expressing ΔEGFR (Fig. 7). Though the increase in phosphorylation of STAT5 is not as large as in cells, it still shows a trend towards increased phosphorylation. These data demonstrate that the signaling events we identified in cultured cells were also present in vivo.

Discussion

ΔEGFR is a potent glioblastoma oncogene but paradoxically it signals at a low level of intensity when compared to acutely stimulated wild-type receptor, although it does so constitutively and without ligand. This suggests that there may be aspects of ΔEGFR signaling that are different from wild-type, and that its downstream targets are particularly important for the promotion of glioma growth and survival. We have used an open, mass spectrometry-based approach to identify tyrosine phosphorylations associated with ΔEGFR, and have identified STAT5 as a new target for this receptor. Our approach was based on using two glioma cell lines, and contrasting samples from cells expressing ΔEGFR with controls, including wild-type EGFR stimulated or not and a kinase inactive mutant of ΔEGFR. We also used a combination of dissociation technologies in the mass spectrometer: both collision induced and electron-transfer dissociations to maximize our yield of post-translational modifications. When we compare phosphopeptides identified with different fragmentation modes, CID identified more unique phosphopeptide ions than in ETD in our study (84% vs 35%). A previous study has found ETD to be much more efficient in identifying phosphopeptides (60% more phosphopeptides identified with ETD)[12]. This difference in our observation may be a consequence of the overall level of phosphorylation which was significantly higher in the above mentioned study due to treatment of cells with a phosphatase inhibitor, resulting in higher amount of phosphopeptides. It is known that ETD fragmentation generates low intensity c and z backbone fragments which can adversely affect identification of peptides. This may have contributed to a lower percentage of unique phosphopeptide identification in our study. But ETD mode identified 16% additional unique phosphopeptides and provided additional information in terms of sequence coverage and localization of PTM site, and so it represented a significant enhancement of our ability to identify phosphorylations.

Our analysis was based on label free quantification, and bioinformatics analysis of the instrument data to increase the yield of peptides that were captured in the analysis. Using this approach we identified 30 tyrosine-phosphorylated peptides that showed statistically significant differences. We most readily identified differences when comparing ΔEGFR to ΔEGFR-ki (n=13), but also saw three peptides with increased phosphorylation in ΔEGFR as compared to EGFR. Of the proteins identified as being phosphorylated by ΔEGFR when compared to ΔEGFR-ki, several had been previously found, including CDC2, Connexin 43, GAB1, cMet (Y1234), MIG6, and SHB [13, 22, 24]. For BCAR1 we saw a decrease, in contrast to the previous study, and we report STAT5, CDK3, CDKN2A, cMet (Y1234,1235), and syndecan 2 as novel. Similarly, when comparing ΔEGFR with EGFR we saw the previously found cMet association with ΔEGFR [13] and for the first time an association between

ΔEGFR and phosphorylation of chemokine orphan receptor 1 and Tensin 3. Also in agreement with previous reports, we saw activation of several MAP kinases by EGFR stimulated by EGF (see Table 1), but did not see these events in cells expressing ΔEGFR [13, 24]. We were able to confirm key phosphorylations, STAT5, c-Met and Gab1 in cultured cells and in xenografts, and Mig6 in cultured cells only. We note that the original observation of increased phosphorylation of STAT5 was made in LNZ308 and LN428 cells, and confirmed with western blot (Figure 6C). In these western blots U87 cells also showed increased phosphorylation of STAT5 but to a lesser extent, and this may explain why in our U87 xenografts we see a more moderate increase in STAT5 phosphorylation; LNZ308 and LN428 do not form intracranial xenografts as reliably as U87 cells.

Quantification of phosphorylation levels both by mass spectrometry and by western blot revealed that in many instances the level of phosphorylation of downstream targets, such as STAT5 and cMet, was just as high in ΔEGFR cells as in cells overexpressing EGFR and acutely stimulated with EGF, despite the lower level of activity attributed to the ΔEGFR. This may indicate that while the level of phosphorylation of the C-terminal domain of the ΔEGFR is lower, this is not reflected in its ability to activate key targets, explaining the apparent paradox of a relatively inactive, yet potent, RTK oncogene.

Pathway analysis of the signaling events we identified in our screen allows us to build a network of interactions based on the published literature (Fig. 8; list of interactions in Supplemental Data, Table S2). The pathway we offer includes proteins seen to have increased tyrosine phosphorylation shown in red, and a few potential linking proteins shown in yellow, which were not observed to be differentially phosphorylated here, but which can be implicated by an established connection between several of the proteins that did emerge in our data. Such a distinct, preferred pathway for ΔEGFR may help in suggesting additional therapeutic targets that could be exploited singly or in combination. Notable in this group is Src, a key node downstream of EGFR and a member of a family of kinases known to be important in glioblastoma biology and a potential target in cancer therapy [25], and a possible link between ΔEGFR and STAT5.

Supplementary Material

Refer to Web version on PubMed Central for supplementary material.

Acknowledgments

We thank the Anthony Bullock III Foundation for their generous support of the proteomics capabilities in the Brain Tumor Center at The University of Texas M. D. Anderson Cancer Center. These studies were supported in part by grants from the National Cancer Institute of the National Institutes of Health: RO1CA108500 (O.B.), P50CA127001 (O.B.), PO1 CAO95616 (W.K.C., F. B.F.) and through The University of Texas M.D. Anderson's Cancer Centre Support Grant CA016672. These studies were also supported by the Goldhirsh Foundation (F.F.). W.K.C. is a Fellow of the National Foundation for Cancer Research. We thank Verlene Henry and Lindsay Holmes of Dept. of Neurosurgey, UT MD Anderson Cancer Center for their help in carrying out animal experiments.

References

1. Comprehensive genomic characterization defines human glioblastoma genes and core pathways. Nature 2008;455(7216):1061–8. [PubMed: 18772890]
2. Wong AJ, Ruppert JM, Bigner SH, Grzeschik CH, Humphrey PA, Bigner DS, Vogelstein B. Structural alterations of the epidermal growth factor receptor gene in human gliomas. Proc.Natl.Acad.Sci.U.S.A 1992;89(7):2965–2969. [PubMed: 1557402]
3. Frederick L, Eley G, Wang XY, James CD. Analysis of genomic rearrangements associated with EGRFvIII expression suggests involvement of Alu repeat elements. Neuro.-oncol 2000;2(3):159–163. [PubMed: 11302336]

4. Chu CT, Everiss KD, Wikstrand CJ, Batra SK, Kung HJ, Bigner DD. Receptor dimerization is not a factor in the signalling activity of a transforming variant epidermal growth factor receptor (EGFRvIII). Biochem.J 1997;324(Pt 3):855–861. [PubMed: 9210410]
5. Huang HS, Nagane M, Klingbeil CK, Lin H, Nishikawa R, Ji XD, Huang CM, Gill GN, Wiley HS, Cavenee WK. The enhanced tumorigenic activity of a mutant epidermal growth factor receptor common in human cancers is mediated by threshold levels of constitutive tyrosine phosphorylation and unattenuated signaling. J.Biol.Chem 1997;272(5):2927–2935. [PubMed: 9006938]
6. Nishikawa R, Ji XD, Harmon RC, Lazar CS, Gill GN, Cavenee WK, Huang HJ. A mutant epidermal growth factor receptor common in human glioma confers enhanced tumorigenicity. Proc.Natl.Acad.Sci.U.S.A 1994;91(16):7727–7731. [PubMed: 8052651]
7. Schmidt MHH, Chen B, Randazzo LM, Bogler O. SETA/CIN85/Ruk and its binding partner AIP1 associate with diverse cytoskeletal elements, including FAKs, and modulate cell adhesion. J Cell Sci 2003;116(14):2845. [PubMed: 12771190]
8. Schmidt MHH, Furnari FB, Cavenee WK, Bogler O. Epidermal growth factor receptor signaling intensity determines intracellular protein interactions, ubiquitination, and internalization. Proc.Natl.Acad.Sci.U.S.A 2003;100(11):6505. [PubMed: 12734385]
9. Cavenee WK. Genetics and new approaches to cancer therapy. Carcinogenesis 2002;23(5):683–6. [PubMed: 12016138]
10. Macek B, Mann M, Olsen JV. Global and site-specific quantitative phosphoproteomics: principles and applications. Annu Rev Pharmacol Toxicol 2009;49:199–221. [PubMed: 18834307]
11. Olsen JV, Blagoev B, Gnad F, Macek B, Kumar C, Mortensen P, Mann M. Global, in vivo, and site-specific phosphorylation dynamics in signaling networks. Cell 2006;127(3):635–48. [PubMed: 17081983]
12. Molina H, Horn DM, Tang N, Mathivanan S, Pandey A. Global proteomic profiling of phosphopeptides using electron transfer dissociation tandem mass spectrometry. Proc Natl Acad Sci U S A 2007;104(7):2199–204. [PubMed: 17287340]
13. Huang PH, Mukasa A, Bonavia R, Flynn RA, Brewer ZE, Cavenee WK, Furnari FB, White FM. Quantitative analysis of EGFRvIII cellular signaling networks reveals a combinatorial therapeutic strategy for glioblastoma. Proc Natl Acad Sci USA 2007;104(31):12867–72. [PubMed: 17646646]
14. Chen B, Borinstein SC, Gillis J, Sykes VW, Bogler O. The glioma-associated protein SETA interacts with AIP1/Alix and ALG-2 and modulates apoptosis in astrocytes. J Biol Chem 2000;275(25):19275–81. [PubMed: 10858458]
15. Baker PR, Medzihradszky KF, Chalkley RJ. Improving software performance for peptide electron transfer dissociation data analysis by implementation of charge state- and sequence-dependent scoring. Mol Cell Proteomics 9(9):1795–803. [PubMed: 20513802]
16. Kandasamy K, Pandey A, Molina H. Evaluation of several MS/MS search algorithms for analysis of spectra derived from electron transfer dissociation experiments. Anal Chem 2009;81(17):7170–80. [PubMed: 19639959]
17. Team, RDC. R: A Language and Environment for Statistical Computing. R Foundation for Statistical Computing; Vienna, Austria: 2009.
18. Pounds S, Morris SW. Estimating the occurrence of false positives and false negatives in microarray studies by approximating and partitioning the empirical distribution of p-values. Bioinformatics 2003;19(10):1236–42. [PubMed: 12835267]
19. Lal S, Lacroix M, Tofilon P, Fuller GN, Sawaya R, Lang FF. An implantable guide-screw system for brain tumor studies in small animals. J Neurosurg 2000;92(2):326–33. [PubMed: 10659021]
20. Molina H, Matthiesen R, Kandasamy K, Pandey A. Comprehensive comparison of collision induced dissociation and electron transfer dissociation. Anal Chem 2008;80(13):4825–35. [PubMed: 18540640]
21. Good DM, Wirtala M, McAlister GC, Coon JJ. Performance characteristics of electron transfer dissociation mass spectrometry. Mol Cell Proteomics 2007;6(11):1942–51. [PubMed: 17673454]
22. Holgado-Madruga M, Emlet DR, Moscatello DK, Godwin AK, Wong AJ. A Grb2-associated docking protein in EGF- and insulin-receptor signalling. Nature 1996;379(6565):560–564. [PubMed: 8596638]

23. Quesnelle KM, Boehm AL, Grandis JR. STAT-mediated EGFR signaling in cancer. J Cell Biochem 2007;102(2):311–9. [PubMed: 17661350]

24. Moscatello DK, Holgado-Madruga M, Emlet DR, Montgomery RB, Wong AJ. Constitutive activation of phosphatidylinositol 3-kinase by a naturally occurring mutant epidermal growth factor receptor. J.Biol.Chem 1998;273(1):200–206. [PubMed: 9417065]

25. Levin VA. Basis and importance of Src as a target in cancer. Cancer Treat Res 2004;119:89–119. [PubMed: 15164875]

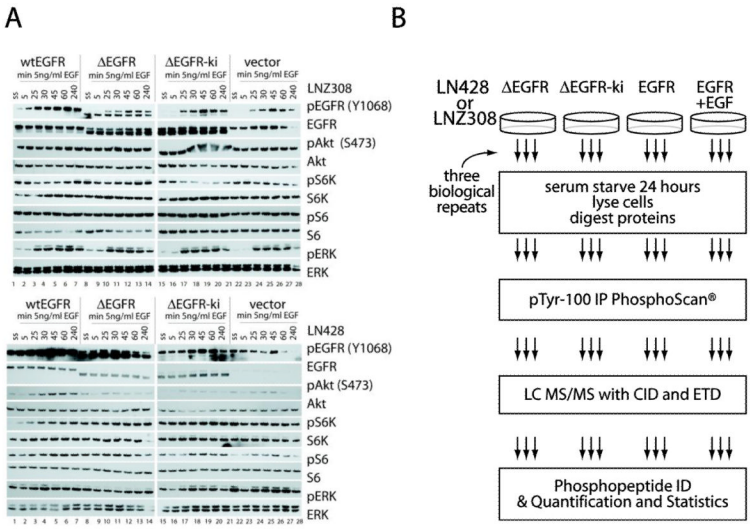

Figure 1. PhosphoScan Analysis of ΔEGFR signaling in two glioma cell lines

(A) Western blot of EGR and PI3K pathway signaling in the cells used for the PhosphoScan analysis. For this analysis, the same lysates were run in parallel on different gels for blotting with the antibodies indicated. (B) Schematic of the PhosphoScan experiment: for each cell line (LNZ308 and LN428) three independent sets of four isolates were prepared (serum starved cells expressing ΔEGFR, ΔEGFR-ki, EGFR and EGFR stimulated with EGF). These were processed for PhosphoScan and analyzed by mass spectrometry.

Figure 2. Quantitative Analysis of phosphopeptides identified and their cluster analysis

(A and B) Graphical representation of differential phosphorylation in three the peptides identified by PhosphoScan. Note that some phosphorylations are represented by more than one peptide in our analysis e.g. Y1197 and Y1172 of EGFR.

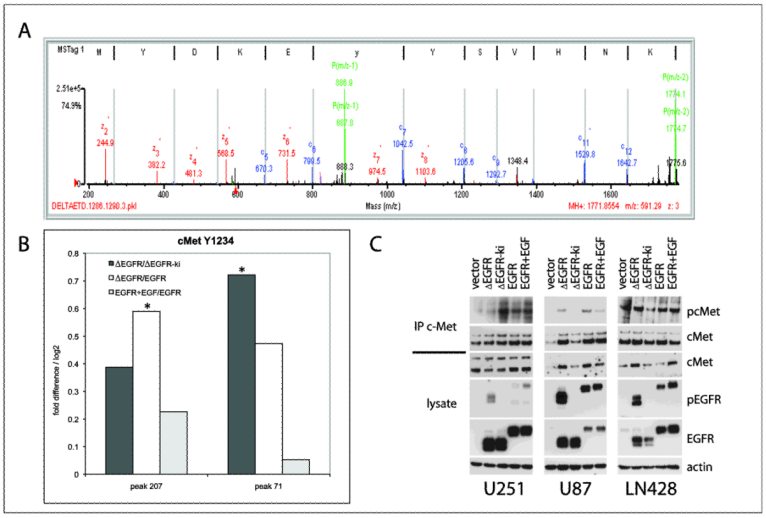

Figure 3. c-Met phosphorylation by ΔEGFR and EGFR in glioma cells

(A) Mass spectrum of c-MET peptide collected in ETD mode, showing Y1234 phosphorylation; c- and z-type ions corresponding to different fragments of the peptide are shown. (B) Fold changes in expression of two different c-MET peptides with Y1234 phosphorylation is shown as difference in Log2 expression values. Expression of both peptides was higher in ΔEGFR expressing cells when compared to EGFR and ΔEGFR-ki expressing cells. (C) Western blot of three glioma cell lines stably expressing ΔEGFR, ΔEGFR-ki, EGFR and EGFR stimulated with EGF showing phosphorylation of cMet (Y1234) in c-Met IPs. It was necessary to immunoprecipitate the c-Met protein before analyzing its phosphorylation status to avoid cross-reaction of the anti-pc-Met (Y1234) antibody with pEGFR.

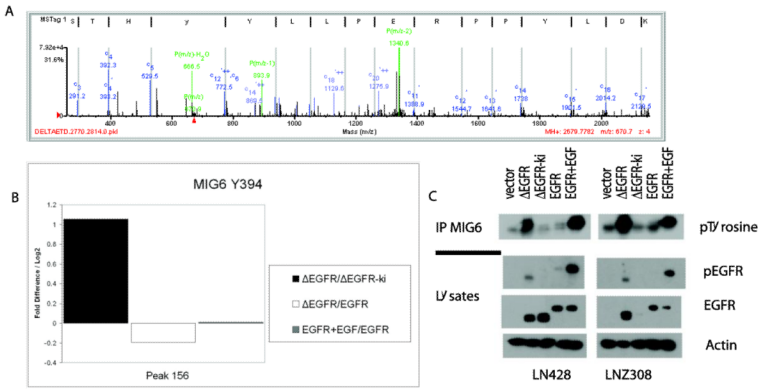

Figure 4. Mig-6 phosphorylation by ΔEGFR and EGFR in glioma cells

(A) Mass spectrum of Mig-6 peptide collected in ETD mode, showing Y394 phosphorylation; c- and z-type ions corresponding to different fragments of the peptide are shown. (B) Fold changes in expression of Mig-6 peptide with Y394 phosphorylation is shown as difference in Log2 expression values. Expression of this peptide was higher in ΔEGFR expressing cells when compared ΔEGFR-ki expressing cells. (C) Western blot of two glioma cell lines stably expressing ΔEGFR, ΔEGFR-ki, EGFR and EGFR stimulated with EGF showing phosphorylation of MIg6 in Mig-6 IPs. It was necessary to immunoprecipitate the Mig6 protein before analyzing its phosphorylation status by anti phosphotyrosine antibody.

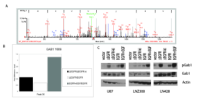

Figure 5. Gab-1 phosphorylation by ΔEGFR and EGFR in glioma cells

(A) Mass spectrum of Gab-1 peptide collected in CID mode, showing Y589 phosphorylation; y-type ions corresponding to different fragments of the peptide are shown. (B) Fold changes in expression of Gab-1 peptide with Y589 phosphorylation is shown as difference in Log2 expression values. Expression of peptide was higher in ΔEGFR expressing cells when compared ΔEGFR-ki and EGFR expressing cells. (C) Western blot of three glioma cell lines stably expressing ΔEGFR, ΔEGFR-ki, EGFR and EGFR stimulated with EGF showing phosphorylation of Gab-1.

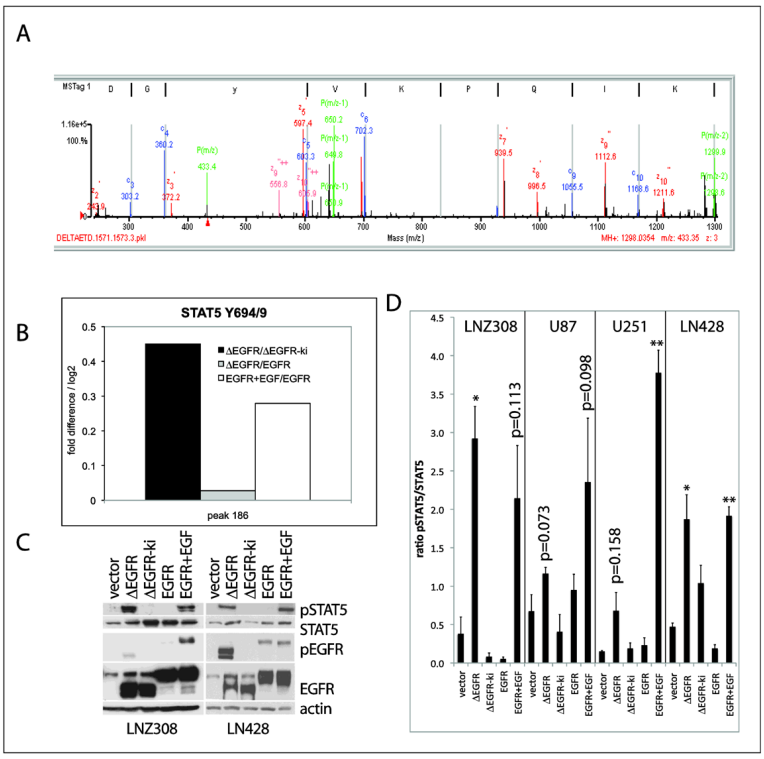

Figure 6. STAT5 phosphorylation is elevated in glioma cells expressing ΔEGFR

(A) Mass spectrum of STAT5 peptide collected in ETD mode showing Y694/9 phosphorylation; c- and z-types of ions corresponding to different fragments of the peptide are shown. (B) Fold changes in expression of the STAT5B peptide with Y694/9 phosphorylation is shown as difference in Log2 expression values. The expression of the Y699 phosphorylated peptide was higher in ΔEGFR expressing cells when compared to ΔEGFR-ki expressing cells. (C) Western blots of the two cell lines used in the PhosphoScan analysis showing the presence of pSTAT5 (Y694/9) when serum starved cells expressed ΔEGFR or expressed EGFR and were stimulated with EGF. (D) Quantification of three (LNZ308, U251 and LN428) or four (U87) western blots as in C, represented as pSTAT5 signal relative to total STAT5 signal, shown as mean and SEM (* $p<0.05$; **$p<0.01$; t-test vs vector).

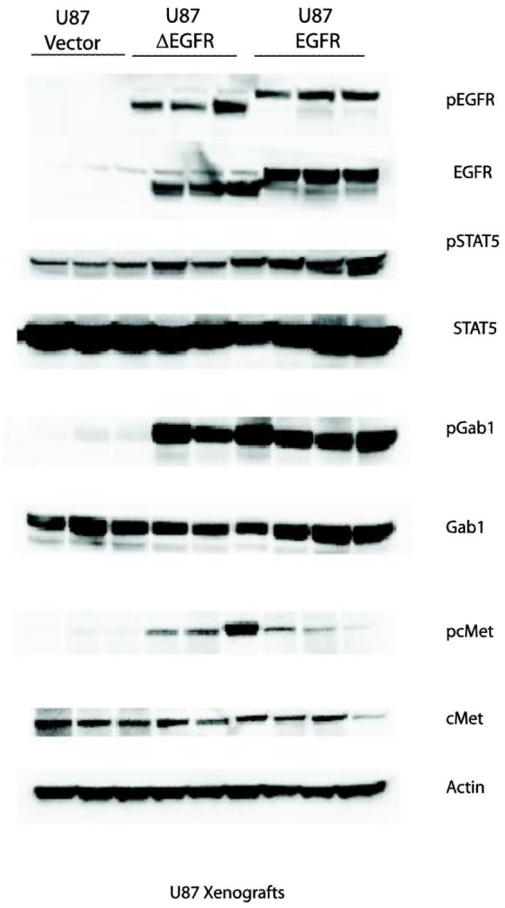

Figure 7. In vivo confirmation of selected phosphorylation events

Nude mice were implanted intracranially with either U87 MG cells with empty vector or U87MG cells over-expressing ΔEGFR or U87MG cells over-expressing EGFR. Tumors formed were harvested after signs of any distress were evident in animals and western blot analysis was done for EGFR, phospho-EGFR (Y1068), cMet, phospho-cMet, STAT5,phospho-STAT5, Gab1 and phospho-Gab1. These western blots show that tumors expressing ΔEGFR and EGFR show greater phosphorylation of cMET, Gab1 and STAT5 phosphorylation. The level of pSTAT5 in ΔEGFR-expressing tumors was 1.5 fold higher when compared to tumors generated with parental U87 cells (p=0.07; t-test).

Figure 8. Pathway analysis of ΔEGFR signaling in glioma cells

Pathway Studio 6 was used to construct a pathway from all phosphoproteins that had a higher signal in ΔEGFR vs ΔEGFR-ki and a $p<0.05$ in statistical analysis (red). The mammalian database was used with protein modification being the only parameter used to connect different protein nodes. Pathway Studio added several intermediate nodes (yellow) to complete the pathway. For more information on the proteins shown in this analysis and their relationship see Supplemental Data, Tables S1 and S2.

Table 1

Tyrosine phosphorylations that show statistically significant change in at least one comparison

Protein Name (alphabetical order)	Phospho Residue(s)	ΔEGFR Vs ΔEGFR-ki	ΔEGFR vs EGFR	EGFR+EGF vs EGFR	Peak(s)
breast cancer anti-estrogen resistance 1	Y267	↓	-	-	346
cell division cycle 2 prot. isoform 1	Y15	↑	-	-	81
chemokine orphan receptor 1 (GPR159)	Y354	-	↑	-	401
connexin 43	Y313	↑	-	-	409
cyclin-dependent kinase 3	Y15	↑	-	-	226
cyclin-dependent kinase inhibitor 2A isoform 1	Y44	-	-	↓	448
dysferlin	Y198	-	↓	↓	297
EGFR isoform a	Y1197	↑	-	-	47,48
EGFR isoform a	Y1172	↑	-	-	49,50
GRB2-associated binding protein 1 isoform a	Y689	↑	-	↑	90
inositol polyphosphate phosphatase-like 1 (SHIP2)	Y986	-	↓		500
male germ cell-associated kinase	Y159	-	-	↑	165
met proto-oncogene precursor	Y1234	↑	↑	-	71,207
met proto-oncogene precursor	Y1234,Y1235	↑	-	-	205
MAPK 1	T185,Y187	-	-	↑	140,249,250
MAPK 3 isoform 1	Y204	-	-	↑	153,257
MAPK 3 isoform 1	T202,Y204	-	-	↑	155
MAPK 7 isoform 1	Y221	-	-	↑	32
MAPK 14 isoform 2	Y182	-	-	↑	33
MAPK 14 isoform 2	T175,Y182	-	↓	-	34
mitogen-inducible gene 6 protein	Y394	↑	-	-	156
NKF3 kinase family member	Y635	-	↓	-	266
Src homology 2 domain containing adaptor protein B	Y268	↑	-	-	2
signal transducer and activator of transcription 5B	Y694	↑	-	-	186
syndecan 2 precursor	Y200	↑	-	-	442

Protein Name (alphabetical order)	Phospho Residue(s)	ΔEGFR Vs ΔEGFR-ki	ΔEGFR vs EGFR	EGFR+EGF vs EGFR	Peak(s)
talin 1	Y1116	-	↓	-	486
tensin 3	Y855	-	↑	-	21
tensin 3	S776,Y780	-	-	↑	175
tensin 3	Y780	↑	-	-	174,268
vimentin	Y38	-	↓	-	509

EGFR= epidermal growth factor receptor; MAPK= mitogen activated protein kinase. (↑ significant increase in phosphorylation level; ↓ significant decrease in phosphorylation level; - No significant change observed; P<0.01). Peak numbers refer to the specific peaks identified by mass spectrometry, and can be used to identify the relevant data in the Supplemental Data Table S1.

Table 2

Comparison of CID and ETD fragmentation in identifying unique phosphopeptide identification

This table shows all the phosphotyrosine-containing peptides identified in our study. These numbers are for unique phosphopeptide ions defined as having unique sequence, charge and post-translational modifications.

	No.	Percentage
Unique phosphpeptide ions identified by both CID and ETD	86	18.45%
Unique phosphpeptide ions identified by CID only	304	65.23%
Unique phosphpeptide ions identified ETD only	76	16.3%
Total	466	100%